Pebble Accretion

Chris W. Ormel

Abstract Pebble accretion refers to the growth of planetary bodies through the accretion of pebble-sized particles. Pebbles are defined in terms of their aerodynamically size τ_s, which describes the level of coupling to the disk gas. Observations confirms the presence of pebble-sized particles in both protoplanetary disks and the early solar system. Pebble accretion proceeds through the settling mechanism, where particles settle to the surface of the planet. This Chapter discusses the key aspects of the pebble accretion framework: the accretion regimes, the planet initiation mass, and the planet isolation masses. The accretion behavior of loosely coupled $\tau_s > 1$ particles, referred to as "large pebbles", is also examined. The pebble accretion probability, ε, is shown to be a useful parameter for evaluating the efficiency of the process, though this quantity is not necessarily high. Distinctions between pebble and planetesimal accretion are outlined. Pebble accretion, in particular, can be a highly effective mechanism in dense rings, as witnessed with ALMA.

Introduction: Pebbles

Pebble accretion is a process that describes the growth of large bodies (planetesimals or planets) by accretion of small, aerodynamically active particles. It should not be confused with processes that describe the formation of macroscopic bodies itself, which could also involve pebble-sized particles. In particular, the streaming instability (or other drag-mediated instabilities) describe how planetesimal size bodies form by concentration and subsequent gravitational collapse. But this is not pebble accretion.

Before introducing pebble accretion we first must clarify what pebbles are in an astrophysical context. I will define

Chris W. Ormel

Department of Astronomy, Tsinghua University, 100084 Beijing, China, e-mail: chrisormel@tsinghua.edu.cn

> Pebbles are aerodynamically active particles that can drift over significant distances within the lifetime of the protoplanetary disk

In the next, I review the observational evidence for the existence of pebble-sized particles in disks and the aerodynamics of particles in gas-rich disks. Then I will intro the key physical underpinning pebble accretion and the framework as it has developed over the past decade.

Observational Evidence for Pebbles in Disks

In protoplanetary disks, pebbles settle to the midplane regions due to the vertical component of the stellar gravity. The midplane regions of the disk would typically be inaccessible with facilities that operate at optical and near-IR wavelengths (including JWST). It is only at radio wavelength that the midplane regions are revealed. Here, ALMA has revolutionized the field by spatially resolving disks, showing a variety of substructure in the forms of spirals, vortices, and, especially, rings. This substructure is best exhibited at continuum wavelengths, which traces the underlying solids population. The prevalence of substructure offers us with the first line of evidence for the dominance of pebble-sized particles in disks. Unless substructure can directly be generated from infalling material (Calcino et al., in prep) only pebble-sized particles would have the aerodynamical properties to migrate over the distances required to display the substructure.

A straightforward example of this argument is that disks tend to be seen significantly smaller in continuum than in the gas (Sanchis et al. 2021). The explanation is that pebble-sized particles have vacated the outer disks, drifting $\sim$10 au inwards. A more subtle example is that pebble-sized particles, would strongly react to any local pressure perturbation, i.e., pebbles pile-up in pressure maxima. Even when the magnitude of the pressure perturbation that lies behind the reversal is small, $|\delta P|/P \ll 1$, it would greatly amplify the imprint on the pebble disk. The at times spectacular substructure seen in ALMA continuum requires aerodynamically active particles.

The second line of evidence for the existence of pebbles, is the spectral dependence of the observed emission I_ν at sub(mm)/radio wavelengths. This dependence arises from the size dependence of the opacity κ_ν—the absorption cross section per unit solid mass. In the Interstellar Medium (ISM), grains are thought to be small, reaching sizes up to $\sim$0.1 μm. At sub(mm) wavelengths the Rayleigh limit is applicable and the opacity decreases with wavelength, $\kappa_\nu \propto \nu^\beta$. In the ISM $\beta \approx 1.7$. On the other hand, particles of size much larger than the wavelength would *not* exhibit a wavelength dependence ($\beta = 0$). Hence, grain growth would manifest itself as a decrease in β.

Therefore, if the emission is optically thin and thermalized the spectral index α (as in $I_\nu \propto \nu^\alpha$) is 1-1 related to β since $I_\nu = \tau_\nu B_\nu(T) = \kappa_\nu \Sigma B_\nu(T)$. If the tempera-

ture is known (and under the optically thin assumption) measuring α informs us on the sizes of the underlying particles. Indeed, studies indicate β values substantially smaller than the ISM value, providing evidence for grain growth to pebble sizes (Testi et al. 2014). Although there are many complicating factors to this simple reasoning (optical depth and scattering effects, temperature dependence, dependence of material properties and internal structure) the consensus is that the change in α reflects grain growth (Sierra et al. 2021; Guerra-Alvarado et al. 2024). The inferred disk mass in pebbles for standard T-Tauri disks are quite small, perhaps only several Earth masses (Ansdell et al. 2017), but it is considerably higher for younger Class 0/I disks (Tychoniec et al. 2020).

Other complementary evidence for the presence of grain growth comes from millimeter polarization measurements in disks (Kataoka et al. 2015; Yang et al. 2016) and from the meteoritic record in the solar system. In the latter, undifferentiated (chondritic) meteorites are often stuffed with chondrules: $\sim 300\,\mu$m-sized particles.

Pebble definition

According to the Udden-Wentworth scale pebbles are particles between 4 and 64 mm in diameter (Williams et al. 2006). Wentworth (1922) further motivates:

> "Pebble is from the Anglo-Saxon papol, which meant something small and round, perhaps akin to the Latin *papula, a pustule*."

More recently, the term pebble has been introduced in the context of pebble accretion (Lambrechts and Johansen 2012). Pebbles in this context are neither defined in terms of size nor necessarily round. Instead, the implied meaning of pebble is aerodynamical: pebbbles are particles that couple in a certain way to the gas.

Particles moving through a gaseous medium experience gas drag. The amount of gas drag is customarily expressed in terms a drag coefficient C_D:

$$\boldsymbol{F}_{\mathrm{drag}} = -\frac{1}{2} C_D A \rho_{\mathrm{gas}} v \boldsymbol{v} \tag{1}$$

where A is the cross-sectional area of the particle, $\boldsymbol{v}$ the velocity of the particle with respect to the gas, and ρ_{gas} its density. The lower the C_D, the more economical your sports car or jet aircraft.

At low densities, there are two notes to make. The first is that the drag coefficient C_D in Eq. (1) is not constant. In the literature one can find expressions for how C_D depends on the flow Reynolds number $\mathrm{Re}_p = 2sv/v_{\mathrm{mol}}$ where v_{mol} is the molecular viscosity and s the particle radius (see e.g., Weidenschilling 1997 for spheres). For $\mathrm{Re}_p < 1$ drag is linear in velocity. In addition, if the distances between gas molecules (their mean free path l_{mfp}) exceeds the particle size s, drag follows the specular reflection limit

$$\boldsymbol{F}_{\text{drag}} = -\frac{4\pi}{3}s^2 \rho_{\text{gas}} v_{\text{th}} \boldsymbol{v} \qquad (s < \frac{9}{4}l_{\text{mfp}}) \tag{2}$$

where $v_{\text{th}} = \sqrt{8kT/\pi m_{\text{gas}}}$ is the gas mean thermal motion. In this limit drag is also linear in velocity. This means that a particle's ==stopping time== $t_{\text{stop}} \equiv mv/|F_D|$ becomes independent of velocity:

$$t_{\text{stop}} = \begin{cases} \dfrac{\rho_\bullet s}{\rho_{\text{gas}} v_{\text{th}}} & s < \frac{9}{4}l_{\text{mfp}} & \text{Epstein} \\[12pt] \dfrac{\rho_\bullet s}{\rho_{\text{gas}} v_{\text{th}}} \left(\dfrac{4s}{9l_{\text{mfp}}} \right) & \frac{9}{4}l_{\text{mfp}} < s < s[\text{Re}_p = 1] & \text{Stokes} \end{cases} \tag{3}$$

The independence of stopping time on velocity is the reason t_{stop} is used to quantify the aerodynamical interaction of a particle. Often the stopping time is nondimensionalized with respect to the orbital frequency:

$$\tau_s = t_{\text{stop}} \Omega_K. \tag{4}$$

Thus, $\tau_s < 1$ indicates particles circularize their motion within one orbital period, while $\tau_s > 1$ particles do not. The latter could be described in the framework of Kepler's orbit with gas drag imposing a perturbative force. For $\tau_s \ll 1$ the Kepler representation becomes meaningless; $\tau_s \ll 1$ particles closely follow any gas motion. We will see below that $\tau_s = 1$ are the fastest drifters. Pebbles are hence defined in terms of the aerodynamical stopping time τ_s. Depending on the situation we may define pebbles as $10^{-2} \leq \tau_s \leq 10^2$ particles or perhaps $10^{-3} \leq \tau_s \leq 10^3$. We will refer to pebbles $\tau_s > 1$ as ==large pebbles==. With this definition, any particle in the absence of gas (such that $\tau_s \to \infty$) is not a pebble.

Drift motions

Protoplanetary disks are supported against the stellar gravity by rotation and pressure P. If rotation would be the only support mechanism (i.e., no pressure gradient) the orbital velocity of the gas would equal the Keplerian velocity $v_{\phi,\text{gas}} = v_K = \sqrt{Gm_\star/r}$. In general, the radial pressure gradient (usually negative) provides some hydrostatic support, such that that the gas moves at a velocity $v_{\phi,\text{gas}} \simeq (1 - \eta)v_K$ where η is defined

$$\eta \equiv -\frac{1}{2\Omega_K^2 r \rho_{\text{gas}}} \frac{\partial P}{\partial r} \sim \frac{P}{v_K^2 \rho_{\text{gas}}} \sim h_{\text{gas}}^2. \tag{5}$$

Here, $\partial P/\partial r$ has been assumed to be some power-law of radius, $h_{\text{gas}} = c_s/v_K$ is the gas aspect ratio, and c_s the isothermal sound speed. Hence, $\eta \ll 1$; the gas rotates at near-Keplerian speeds with a departing from Keplerian motion by $\eta v_K \sim 10-100\,\text{m}\,\text{s}^{-1}$.
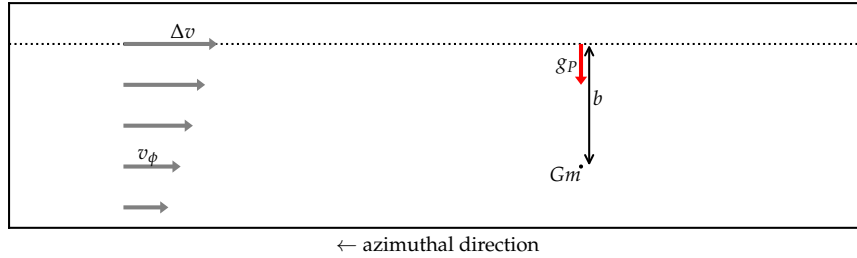
$\leftarrow$ azimuthal direction

Fig. 1 Geometry of the encounter between planet and pebble. The planet moves on a circular orbit in the positive azimuthal direction (leftwards), facing pebbles at a relative velocity v_ϕ—the headwind term. For large impact parameters b the approach velocity Δv is determined by the Keplerian shear. In reality, the approach velocity Δv could also have contributions from v_r, planet eccentricity, and turbulence. At closest approach, the pebble experiences a gravitational acceleration $g_P = Gm/b^2$.

Particles do not feel the gas pressure ($\rho_\bullet \gg \rho_{\mathrm{gas}}$) but they do interact with the gas aerodynamically through drag forces. Gas friction extracts angular momentum from the particles, which therefore tend to drift in radially. Solving for the steady solutions to the Euler equations for gas and particles simultaneously, we find that the drift velocities, in a frame co-moving at the Keplerian orbital velocity are (Nakagawa et al. 1986):

$$v_r = -\frac{2\tau_s}{\tau_s^2 + (1 + Z_{\mathrm{mid}})^2}\eta v_K; \qquad v_\phi = -\frac{(1 + Z_{\mathrm{mid}})}{\tau_s^2 + (1 + Z_{\mathrm{mid}})^2}\eta v_K \qquad (6)$$

where Z_{mid} is the local (midplane) solids-to-gas ratio. Since we will typically assume in this chapter that a planet moves on a circular orbit these are the velocities at which the planet faces the pebbles (see Fig. 1). For small τ_s and $Z_{\mathrm{mid}} \approx 0$ we have that $v_\phi \simeq -\eta v_K$, which expresses that pebbles move along with the gas, and $v_r \simeq -2\eta v_K \tau_s$. The radial drift peaks at $\tau_s = 1$ at which point the drift timescale $t_{\mathrm{drift}} = r/|v_r| \sim 1/\eta\Omega_K$, is just several hundreds of orbital periods. The drift velocities decrease for either $\tau_s \gg 1$ or $Z_{\mathrm{mid}} \gg 1$. In the case where $\tau_s < 1$ but $Z_{\mathrm{mid}} \gg 1$ this happens because the tightly-coupled particles drag the gas along to Keplerian rotation.

The physics of pebble accretion

I will give two definitions of pebble accretion:

1. Pebble accretion is an accretion mechanism where a planet accretes pebble—particles that drift significantly (as defined above).
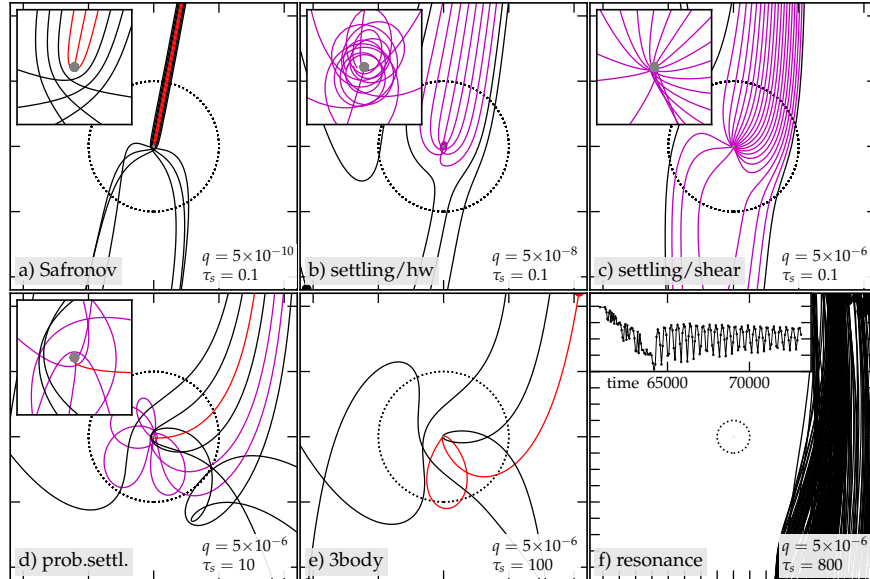
Fig. 2 Trajectories of pebbles with aerodynamical size τ_s in a frame co-moving with the planet of mass $q = m/m_\star$ on a circular orbit. Trajectories in red indicate ballistic accretion: particles hit the surface of the planet (here taken to be $R/R_h = 5 \times 10^{-3}$). Trajectories in purple indicate settling: these particles would be captured in the Hill radius and be accreted even when $R \rightarrow 0$. *Technical notes:* The gas flow pattern is assumed to be unaffected by the planet. Dotted circle denotes the Hill radius and tick marks are also separated by $1\,R_H$. Particles are launched from a ring outside the planet's orbit at fixed azimuthal intervals. Therefore, each trajectory carries the same amount of the pebble flux. c) some particles accrete from the back. e) Two trajectories are shown; the non-accreting particle re-enters the Hill radius three times. f) One particle trajectory is shown, which get trapped in resonance. The inset shows the distance to successive conjunctions as function of time.

2. Like above, but where in addition the pebbles are *captured* in the planet's gravitational well and *settle* to the surface of the planet

    The second definition is usually what is understood with "pebble accretion". I will describe these settling trajectories first, before outlining the region in the planet mass–pebble size parameter space where we can find these.

Settling trajectories

The region about the planet dominated by its gravity, rather than that of the star, is given by its <mark>Hill radius</mark>

$$R_H = r \left(\frac{m}{3m_\star} \right)^{1/3} \tag{7}$$

where m is the mass of the planet and r the distance to the star of mass $m_\star$. Pebble accretion may be defined as *capture* of particles within the Hill sphere. Such trajectories are referred to as settling trajectories and pebble accretion in its narrow sense is synonymous with this capture mechanism. This contrast ballistic interactions, which rely on hitting a surface. Ballistic trajectories can graze the planet's surface, but such close encounters are absent if the accretion proceeds by settling. The difference between settling and ballistic accretion paths is illustrated in Fig. 2 with purple and red trajectories, respectively, for a variety of planet masses and particle stopping times. Would the surface disappear (e.g., the gravitating body shrinks to a point mass), ballistic accretion vanishes (in Fig. 2, trajectories in red would then exit the Hill radius). Particles accreted through the settling mechanism, on the other hand, would be unaffected. This definition is not only academic. In the Hill units adopted in Fig. 2, the planets surface, R/R_H, shrinks with stellar orbital radius r and most ballistic accretion vanishes (red trajectories turn black). Pebble accretion is therefore comparatively more relevant in the outer disk.

Gas drag balancing gravity will result in a terminal velocity—the settling velocity—equal to $v_{\text{settl}} = g_P t_{\text{stop}}$, where g_P is the gravitational acceleration of the planet. For pebbles to settle towards the planet, the settling timescale

$$t_{\text{settl}} = \frac{b}{v_{\text{settl}}} = \frac{b^3}{Gmt_{\text{stop}}} \tag{8}$$

with b the impact parameter (see Fig. 1), must be shorter than the duration of the encounter, t_{enc}. The latter could be estimated as $\sim b/\Delta v$ where Δv is the velocity at which a pebble approaches the planet. Equating t_{settl} and t_{enc} we readily find the accretion rate

$$\dot{m}_{\text{3D}} \sim \rho b^2 \Delta v \sim Gmt_{\text{stop}}\rho. \tag{9}$$

This is the 3D limit, because we assumed that particles are homogeneously distributed over the entire cross section $\sim b^2$ at density ρ. Remarkably, $\dot{m}_{\text{3d}}$ is independent of the relative velocity Δv. If the particle layer is sufficiently settled with respect to the impact parameter b, the accretion becomes 2D. In that case we solve for $b(\Delta v)$ first to obtain:

$$\dot{m}_{\text{2d}} \sim b\Delta v \Sigma \sim \sqrt{\frac{Gmt_{\text{stop}}}{\Delta v}} \Delta v \Sigma \sim \sqrt{Gmt_{\text{stop}}\Delta v}\Sigma. \tag{10}$$

Note that we have not specified the source of the approach velocity Δv; it can be due to the drift of the particles or the eccentricity of the planet (or something else). The limit where Δv is determined by the pebble drift, $\Delta v \sim \eta v_K$, is referred to as the headwind limit or the Bondi limit. If, on the other hand, the approach velocity is given by the Keplerian shear, $\Delta v \sim b\Omega$ and $t_{\text{enc}} \sim \Omega^{-1}$, we instead obtain

$$\dot{m}_{\text{2d}-\text{shear}} \sim \left(\frac{Gm t_{\text{stop}}}{\Omega} \right)^{2/3} \Omega \Sigma \sim R_h^2 \Omega \tau_s^{2/3} \Sigma. \tag{11}$$

which is known as the shear limit or Hill limit. In Fig. 2 panels (b) and (c) illustrate pebble accretion in the headwind and shear limits, respectively. It is in the 2D/shear limit where accretion rates peak. For $\tau_s \sim 0.1$–1 almost all particles entering the Hill radius are accreted!

There is an important caveat to the expressions derived above. In these, we have assumed particles approach their terminal settling velocities. In reality, this takes a time t_{stop}. This implies that the duration of the interaction should be longer than the stopping time, $t_{\text{enc}} > t_{\text{stop}}$—the settling condition. If the encounter time is determined by the approach velocity Δv and b by Eq. (10), the condition $t_{\text{stop}} < b/\Delta v$ translates into

$$t_{\text{stop}} \lesssim \frac{Gm}{(\Delta v)^3} \quad \text{or} \quad \tau_s \lesssim \frac{m}{m_\star} \left(\frac{\Delta v}{v_K} \right)^{-3} \quad \text{or} \quad m \gtrsim m_* \equiv \left(\frac{\Delta v}{v_K} \right)^3 \tau_s m_\star. \tag{12}$$

Planets of mass $\ll m_*$ cannot accrete pebbles through the settling mechanism (Fig. 2a). In addition, for pebbles $\tau_s \geq 1$ the encounter time is $\sim \Omega^{-1} < t_{\text{stop}}$ and therefore the settling condition generally fails.

Pebble accretion parameter space

Figure 3 presents an overview of pairwise accretion mechanisms operating in the parameter space of planet mass and pebble aerodynamical size. In Fig. 3 and many other figures I assume that a (proto)planet of mass m (y-axis) interacts with pebbles of Stokes number τ_s (x-axis) that drift inwards according to the free drift expressions (Eq. 6). The regimes boundaries are indicative as we have not accounted for transition effects or order-of-unity factors; they could easily shift by an order of magnitude. The line style indicates the nature of the transition with thick solid lines indicating abrupt transition (e.g., ballistic to settling), dashed lines gradual transitions (e.g., the 3D-to-2D transitions), and dotted line "fluid" transitions, meaning that two distinct accretion mechanisms operate on both sides of the stated boundary. The domain of pebble accretion (as per the settling mechanism) resides within the thick lines. The thick dashed line arises because ballistic trajectories are continues across the line, while settling trajectories are not.

In the small pebble limit ($\tau_s < 1$) pebble accretion is limited by the pebble isolation mass from above and by the settling condition (Eq. 12) from below. Here settling encounters abruptly give way to the usual 2-body ballistic accretion (Fig. 2a):

$$\dot{m} = \pi R^2 (1 + \Theta) \Delta v \rho = \pi R^2 \left(1 + \frac{2Gm}{R(\Delta v)^2} \right) \Delta v \rho \tag{13}$$
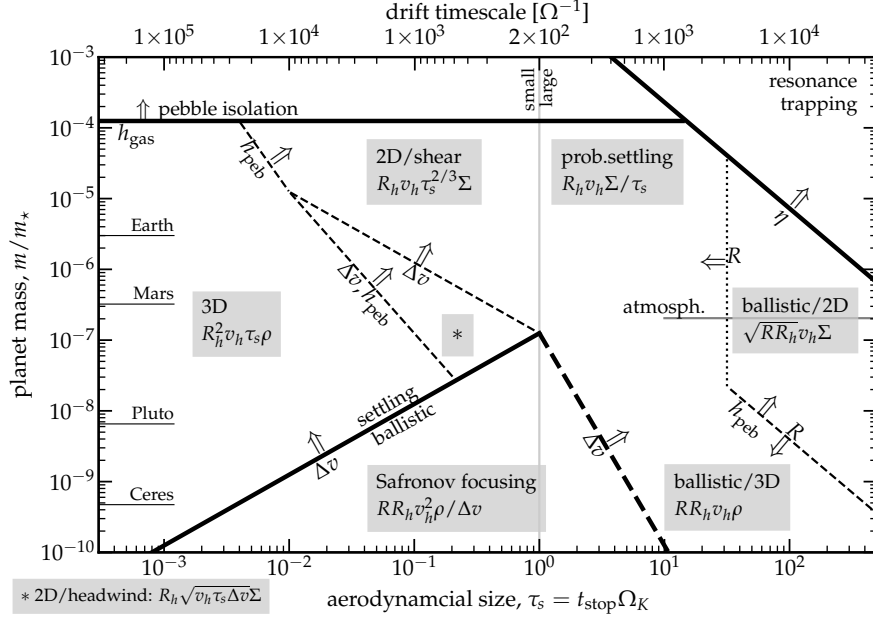
Fig. 3 Schematic summarizing accretion mechanisms and their accretion rates $\dot{m}$. The leading terms in the expression for $\dot{m}$ for each of the regimes are given. Boundaries between accretion regimes are indicative and will in reality shift when accounting for order-of-unity factors. It is further indicated how the regime boundaries shift upon change of the parameters Δv, h_{peb}, R, and η. Here, R is the physical radius of a body, R_h its Hill radius, $v_h = R_h \Omega$, Δv the approach velocity between planet and pebble, and h_{peb} the pebble scaleheight. The figure has been drawn for $\eta = 5 \times 10^{-3}$, $R/R_h = 10^{-3}$, h_{peb} following Eq. (27) with $\delta_z = 10^{-4}$ and a disk aspect ratio of $h_{gas} = 0.05$. Thick lines indicate abrupt changes in the accretion rate (e.g., onset of pebble accretion, pebble isolation, and resonances). The dotted line at $\tau_s \approx 30$ indicates that settling and ballistic accretion mechanisms operate on each side of the line.

where Θ is the gravitational focusing factor. The corresponding expression in Fig. 3 only keeps the part including Θ and is written in Hill units where $Gm = 3R_H v_H^2$ and $v_H = R_H \Omega$. This "Safronov focusing" is central to many studies about planetesimal accretion where Δv arises from the eccentricity of the planetesimal bodies. In the pebble case Δv is given by Eq. (6) and independent of planet mass.

We refer to pebbles with $\tau_s > 1$ as large pebbles. By definition, large pebbles have stopping times longer than an orbital time and do not generally obey the settling condition. Nevertheless, for not too large τ_s accretion can still proceed and in fact be dominated by settling (Fig. 2d). While most particles get ejected from the Hill radius *some* fail to escape the Hill radius to settle towards the planet. The efficiency of this *probabilistic settling* decreases with τ_s^{-1}. This implies that ballistic accretion, which operates in the 2D equivalent of Eq. (13) will gradually overtake settling at $\tau_s \sim \sqrt{R_h/R}$. The transition is gradual; both accretion types co-exists for $\tau_s > 1$ particles (as illustrated in Fig. 2d).

Table 1 Asymptotic expressions for pebble accretion rates $\mathcal{R}_{\mathrm{peb}}$ and efficiencies ε in the 2D and 3D limits.

Δv	$\mathcal{R}_{2\mathrm{d}}$	$\varepsilon_{2\mathrm{d}}$	$\mathcal{R}_{3\mathrm{d}}$	$\varepsilon_{3\mathrm{d}}$
– headwind	$4.0(\eta\tau_s q)^{1/2}$	$0.32(q/\eta\tau_s)^{1/2}$		
– eccentricity	$3.5(e\tau_s q)^{1/2}$	$0.28(eq/\eta^2\tau_s)^{1/2}$	$4.9\tau_s q/h_{\mathrm{peb}}$	$0.39q/\eta h_{\mathrm{peb}}$
– shear	$2.9(\tau_s q)^{2/3}$	$0.23(q^2/\eta^3\tau_s)^{1/3}$		

Notes. Normalized accretion rates, $\mathcal{R} = \dot{m}/\Sigma r^2\Omega$, are given in terms of: e (*planet* eccentricity), h_{peb} pebble scaleheight, η (Eq. 5), $q = m/m_\star$, $\tau_s = t_{\mathrm{stop}}\Omega$ (aerodynamical size). Expressions follow Liu and Ormel (2018) and Ormel and Liu (2018). Expressions valid only for $\tau_s \leq 1$ and masses above m_*. In the 2D limit the expression evaluating to the largest number has precedence, while for the combined $\dot{m}$ Eq. (16) can be used. In the 3D limit, expressions are independent of Δv. In terms of pebble density (ρ) the accretion rate reads $\dot{m} = 12\tau_s q(\rho r^3\Omega)$.

Accretion can be boosted greatly by the emergence of planet atmospheres. This occurs when the surface escape velocity exceeds the thermal velocity of the gas or when the Bondi radius

$$R_B = \frac{Gm}{kT/m_{\mathrm{gas}}} \tag{14}$$

exceeds R. The pre-planetary atmosphere is connected to the disk but is denser than the disk gas. This opens up the possibility for larger particles to be captured. I will nonetheless refer to this type of accretion as ballistic, because a planet's atmosphere is after all connected to the planet. The interaction can then be described with an atmosphere-enhanced capture radius $R_{\mathrm{cap}}(m, \tau_s, \dots)$ replacing the physical radius (Inaba and Ikoma 2003).

Larger pebbles are even less influenced by gas and drift slowly towards the planet. As they approach, they experience long-range gravitational interactions with the planet they approach. The inward drift can then be offset by resonant repulsion. These pebbles are small enough to drift over significant distances but sufficiently large to be captured in mean motion resonances.

The pebble accretion framework

I will discuss here the key elements that make up the pebble accretion framework. These include: accretion rates in the small and large pebble regimes, the pebble isolation and initiation masses.

Pebble accretion rates ($\tau_s < 1$)

Pebble accretion rates for $\tau_s < 1$ particles are compiled in Table 1. These are given in non-dimensionless form with the accretion rate expressed in units of $\Sigma r^2\Omega$. The

prefactors have been obtained from three-body simulations carried out by Liu and Ormel (2018) and Ormel and Liu (2018) and are valid in the stated asymptotic limits. In the 2D limit, accretion rates depend on the relative velocity Δv, which can be due to the headwind of the pebbles, the shear in the disk, or the eccentricity of the planet (whichever is highest). In the 3D limit, accretion rates are independent of Δv but do depend on the scaleheight of the pebbles (or aspect ratio h_{peb}). If the planet is on an inclined orbit, such that the magnitude of the vertical oscillations exceed the pebble scaleheight, h_{peb} should be replaced by the planet inclination i.

In the 2D limit the pebble accretion rate that materializes is the maximum of the headwind, eccentricity, and shear limits. For the headwind and eccentricity limits, rates scale with the square-root of velocity (η or e), reflecting a higher supply rate of pebbles. But this comes at the expense of a higher initiation mass (Eq. (12)). Accretion rates are the highest in the 2D, shear limit. Converting to a growth timescale, we find:

$$t_{\text{grw}}^{\text{2d/shear}} = 2 \times 10^4 \, \text{yr} \, \left(\frac{m}{m_\oplus} \right)^{1/3} \left(\frac{m_\star}{m_\odot} \right)^{-5/6} \left(\frac{\tau_s}{0.01} \right)^{-2/3} \left(\frac{\Sigma r^2 / m_\star}{10^{-5}} \right)^{-1} \left(\frac{r}{5 \, \text{au}} \right)^{3/2}.$$
(15)

It is clear that if Eq. (15) materializes, protoplanets can easily grow to the runaway gas accretion threshold mass. The "problem" with these high accretion rates is that the local reservoir of pebbles will be quickly emptied and need to be resupplied from the outer disk. For these reasons, it is more useful to express these rates in terms of an accretion probability ε (see below).

Table 1 shows that none of the pebble accretion rates are superlinear with mass q. Two equal-mass embryos will grow similarly in terms of mass, a situation resembling of oligarchic growth rather than runaway growth. However, runaway growth effects (i.e., one body outcompetes another one in terms of growth) can yet occur, e.g., when the two bodies are on opposite sides of the R_{init} threshold or in rings, where competitors can be scattered out of the pebble feeding zone.

Modulation factors In reality transitions are smooth. Ormel and Liu (2018) found that the combined rate can be well represented from the respective 2D and 3D expressions

$$\dot{m} = \left(\dot{m}_{\text{2D}}^{-2} + \dot{m}_{\text{3D}}^{-2} \right)^{-0.5}.$$
(16)

In addition, the initiation of pebble accretion around the mass m_* has been fitted by a modulation factor:

$$f_{\text{set}} = \exp \left[-0.5 \left(\frac{\Delta v}{v_*} \right)^2 \right] = \exp \left[-0.5 \left(\frac{m_*}{m} \right)^{2/3} \right]$$
(17)

where $v_* = (q/\tau_s)^{1/3} v_K$ and m_* was defined in Eq. (12) (Ormel and Klahr 2010; Liu and Ormel 2018). 2D rates should be multiplied by f_{set} and 3D rates by f_{set}^2.

A further modulation occurs when pebbles exhibit a size distribution, such that the net accretion rate will be averaged over a particle size distribution. In particular, a planet accreting pebbles of different stopping time may have its mass simultane-

ously below (for large τ_s) or above (for small τ_s) the initiation mass m_* (Lyra et al. 2023). Accounting for a size distribution will hence ameliorate the transition onset of pebble accretion. Turbulence, in which Δv follows a distribution, will have a similar effect (Ormel and Liu 2018).

Pebble initiation mass

A characteristic feature of pebble accretion is that it is abruptly initiated at a mass m_{init} (Eq. 12). If we divide the accretion rates across the pebble accretion initiation line (Fig. 3) we obtain, in the 3D limit:

$$\frac{\dot{m}_{\mathrm{PA,3d}}}{\dot{m}_{\mathrm{Safr}}} \sim \frac{\Delta v}{R_{\mathrm{init}}\Omega}\tau_s \sim \frac{\tau_s^{2/3}}{\alpha_R} \tag{18}$$

where in the last step we used $\alpha_R = R/R_{\mathrm{Hill}}$ to express R_{init} in terms of mass (m_{init}) and then inserted Eq. (12) for m_{init}. This expression illustrates that pebble accretion (by settling) boost accretion rates by factors 10 to 100 and in particular in the outer disk regions where α_R is small. By fitting directly for the intersection of ballistic and settling encounters, Visser and Ormel (2016) found the crossover point to lie at

$$R_{\mathrm{init}} \approx 450\,\mathrm{km}\,\frac{\Delta v}{50\,\mathrm{m\,s^{-1}}}\left(\frac{\rho_\bullet}{1\,\mathrm{g\,cm^{-3}}}\right)^{-0.36}\left(\frac{r}{\mathrm{au}}\right)^{0.42}\left(\frac{m_\star}{m_\odot}\right)^{-0.14}\tau_s^{0.28} \tag{19}$$

where $\rho_\bullet$ is the internal density of the planetesimal. At $m = m_{\mathrm{init}}$, the mass corresponding to R_{init}, accretion rates will steeply rise, until pebble accretion is fully activated at $m \sim m_*$ (Eq. 12).

Planetesimals must exceed R_{init} in order to enter the pebble accretion regime. Bodies that satisfy the constraint could rapidly grow to much larger sizes, rendering the planetesimal distribution bimodal. Conversely, if no single planetesimal exceeds the initiation threshold, planetesimals should grow by other, slower processes—either by ballistic accretion of pebbles or traditional planetesimal-driven accretion. This constraint is particularly severe for the outer disk, because R_{init} may easily be as large as Pluto and alternative mechanism are also slow. Frequently, planet population synthesis models sidestep the initiation threshold condition by starting with a sufficiently high seed mass that already accrete pebbles in the 2D limit (e.g. Johansen et al. 2019; Schneider and Bitsch 2021). However, the origin of these massive seeds is a critical issue in pebble accretion studies, as it is in planetesimal population synthesis.

The situation changes when Δv is small. In Eq. (19) we took Δv consistent with a smooth disk. However, in case of a pressure gradient (low η) or a particle pileup (or traffic jam; $Z_{\mathrm{mid}} \gg 1$) Δv can be much lower (Eq. 6). Under these conditions, the issues posed by the initiation threshold are largely alleviated, allowing growth to proceed more rapidly (see below).

Pebble isolation mass

The inward drift of pebbles exterior to a planet's orbit is driven by the negative pressure gradient in the disk. When the pressure gradient reverses, the pebbles flow terminate. Pressure reversals can be due to disk-related processes, but the planet can also induced them. As it opens a gap in the disk, a (positive) pressure gradient (negative η) develops exterior to the planet, such that pebbles' drift velocity would become positive. Hence, pebbles pile up at the location where the contribution of the planet-induced (positive) pressure gradient and the disk-induced (negative) pressure gradient meet.

The typical scale for gap opening is set when the Hill radius of the planet exceeds the disk scaleheight, which translates into $m \sim h_{\mathrm{gas}}^3 m_\star$. Hence, we write

$$m_{\mathrm{iso}} = 42\, m_\oplus \left(\frac{h}{0.05} \right)^3 \left(\frac{m_\star}{m_\odot} \right) f_{\mathrm{fit}} f_{\mathrm{diff}}. \tag{20}$$

Here f_{fit} is a numerically-obtained modulation function that accounts for effects of disk viscosity and the background pressure gradient (Bitsch et al. 2018)

$$f_{\mathrm{fit}} = 0.6 \left(0.66 + 0.34 \left(\frac{-3}{\log_{10} \alpha_\nu} \right)^4 \right) \left(0.58 - 0.17 \left(\frac{\partial \log P}{\partial \log r} \right)_{\mathrm{disk}} \right). \tag{21}$$

When disks are more viscous or the background pressure gradient is steeper, a gap is harder to open and the pebble isolation mass is larger. The term f_{diff} accounts for the diffusive nature of the dust particles' motions in turbulent flows. At this stage a planet does not fully open a gap, allowing small particles to filter through along with the gas. According to Ataiee et al. (2018), this increases the pebble isolation mass by an amount

$$f_{\mathrm{diff}} = 1 + 0.2 \left(\frac{\sqrt{\alpha_T}}{h_{\mathrm{gas}}} \sqrt{4 + 1/\tau_s^2} \right)^{0.7} \tag{22}$$

Large Pebble accretion ($\tau_s > 1$)

It is commonly believed that growing particles will hit a growth or drift barrier, preventing them from exceeding $\tau_s = 1$ (e.g. Birnstiel et al. 2012). Still $\tau_s > 1$ pebbles can occur in a variety of situations. They could result from collisions between planetesimal bodies. Due to the weaker gravitational bonding of smaller bodies, a collisional cascade could be triggered, grinding a significant fraction of the mass down to particle sizes small enough for gas drag to become effective. Kobayashi et al. (2011) estimate this "fragment size" at $\tau_s \sim 20$ dependent on planet mass, location, and material properties. In addition, small pebbles can become aerodynamically large when the gas depletes, i.e., during disk dispersal or when outgassing occurs
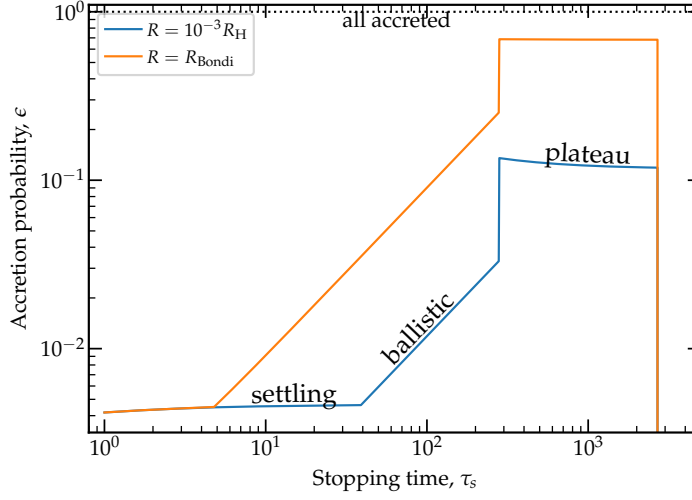
Fig. 4 Probability that a drifting pebble gets accreted for large pebbles ($\tau_s > 1$) with $q = 10^{-6}$, $h_{\mathrm{gas}} = 0.05$ and $\eta = 5 \times 10^{-3}$. Curves follow expressions by Huang and Ormel (2023). The orange curve indicate the enhanced accretion probability due to the atmospheres, which may extend up to the Bondi limit (the exact enhancement depends on the atmosphere model). Beyond $\tau_s \approx 3,000$ pebbles are captured in resonances.

in debris disks. It is therefore meaningful to characterize the accretion properties of large pebbles.

Like small pebbles, we define large pebbles as freely drifting particles (Eq. (6)), ignoring perturbation from bodies other than the planet. Recently, Huang and Ormel (2023) conducted three-body integrations (star, planet, and pebble) within the large pebble accretion regime, employing a global reference frame. These integrations directly determine whether the pebble is accreted by the planet or continues to drifting inwards, i.e., we obtain the accretion probability ε. The advantage of employing a global setup over a local one is that it prevents double (or multiple) counting of accreting pebbles. For example, when $v_r \to 0$ the same pebble could repeatedly enter the planet Hill radius. However, in the local setup, unless care is taken, there is no difference between these multiple encounters. Additionally, in the global frame the resonant forcing of the pebbles by the planet can be followed.

Figure 4 presents a summary of the findings by Huang and Ormel (2023). The probability of getting trapped in the Hill radius by the settling mechanism is approximately $\propto \tau_s^{-1}$ reflecting the amount of energy dissipated within the Hill radius. At small τ_s, the accretion *probability* is therefore constant, because the reduction in the accretion rate is compensated by a slower drift. On the other hand, ballistic accretion rates stay constant with τ_s and in fact may increase greatly due to atmospheres (see below). Huang and Ormel (2023) found that the standard Safronov accretion rate

$$\dot{m}^{2\mathrm{d}} = 2R\Delta v \sqrt{1 + \frac{v_{\mathrm{esc}}^2}{\Delta v^2}} \Sigma \qquad (23)$$

fit their simulated data well. Then, with increasing τ_s drift speeds become so slow that pebbles are guaranteed to enter the Hill radius. If not accreted at first instance, a pebble may reenter the Hill radius multiple times unless it either gets accreted or it is scattered to the inner disk. This results in a fixed accretion probability ε, referred to as the "plateau".

Finally, for even larger τ_s particles end up in a first-order mean motion resonance (at period ratios $j+1{:}j$ with respect to the planet) and will no longer approach the planet. Here, the inward radial drift is compensated by the secular repulsion of the planet (Hasegawa and Nakazawa 1990; Muto and Inutsuka 2009). The threshold stopping time τ_{res} above which pebbles are captured in resonance depends on whether gas damping is "strong" or "weak". The weak limit, where the pebble will develop an eccentricity between successive conjunctions, usually applies for larger planet masses (as in Fig. 4). Importantly, the presence of a resonance barrier does not preclude accretion. As already noted by Weidenschilling and Davis (1985) particles trapped in these high-j resonances would collide and fragment to smaller sizes. In fact pebbles above τ_{res} will be accreted ballistically, aided by an atmosphere.

Atmospheres For planets with $R_B > R$, it has long been recognized that their atmospheres' can trap planetesimal bodies. Inaba and Ikoma (2003) showed that bodies impacting the planet at distance R_c, where the gas density $\rho(R_c)$ has been elevated due to the atmospheres, will lose enough energy to become trapped in the Hill sphere, when

$$\rho(R_c)R_H \gtrsim \frac{6+e_H^2}{9}s\rho_\bullet \tag{24}$$

where e_H is the Hill velocity (See Okamura and Kobayashi 2021 for up-to-date discussion). If this criterion is satisfied we can simply replace R_c for the planet's physical radius (R) in all preceeding expressions. Compared to planetesimals, large pebbles have lower s and e_H. Therefore, Eq. (24) suggests that ballistic accretion rates for large pebbles would be greatly elevated, with R_c increasing up to the Bondi radius (see Fig. 4). Accretion of large pebbles can be extremely efficient.

Miscellaneous points

There are other important facets to pebble accretion, which I will briefly touch on for completeness

Flow isolation The presence of a planet will alter the flow pattern of the gas in its vicinity, with the horseshoe motion a well-known consequence. The deviation from the unperturbed flow pattern becomes particular pronounced at the scale of the Bondi radius R_b, i.e., when atmospheres appear. 3D hydrodynamical simulations typically show gas inflowing from the polar regions and an outflow of gas in the midplane (Ormel et al. 2015; Cimerman et al. 2017; Kuwahara and Kurokawa 2024). Small pebbles ($\tau_s \ll 1$) that reside in the midplane could therefore be aerodynamically deflected away from the planet if R_b exceeds the pebble accretion capture

radius is. This flow isolation therefore occurs in the limit of small τ_s and large planets, although results are rather dependent on the gas drag law (Epstein or Stokes), gas thermodynamics (cooling), and the value of the radial pressure gradient (headwind or shear) Kuwahara and Kurokawa (2020a,b). Kuwahara and Kurokawa (2020b) find that pebbles of $\tau_s \lesssim 10^{-3}$ generally avoid accretion for planets more massive than $R_b/H > 0.03$.

Spin Particles that impact another body transfer angular momentum, contributing to its spin. While the spin of giant planets is believed to originate from gas accreted through a circumplanetary disk, the origin of the spin of the terrestrial bodies in the solar system is unclear. If the planetary bodies accreted mostly planetesimals, the imparted angular momentum would be insufficient (Dones and Tremaine 1993). In contrast, accretion of pebbles transfers more substantial amounts of angular momentum (Visser et al. 2020). However, once an atmospheres forms its rotation is expected to become clearly prograde, which would drag the pebbles along (Takaoka et al. 2023).

Pebble Torque Planets migrate in disks due to an axisymmetric distribution of density. Even though solids constitute only $\sim 1\%$ of the mass, they can nevertheless induce an asymmetry that makes the net torque from solids comparable to the better-known gas-induced torques (Benítez-Llambay and Pessah 2018). In particular, pebbles are typically accreted from the front of the planet creating a solid deficit behind the planet's orbit (see Fig. 2b). This results in a positive and significant torque acting on the planet (Chrenko et al. 2024).

Envelope enrichment and compositional implications A misconception of the core accretion model is that all accreted solids assemble in the central "core" of the planet. In reality, solids—especially slowly settling pebbles—can undergo thermal ablation in the hot envelopes surrounding accreting protoplanets (Venturini et al. 2015; Brouwers et al. 2018). If the sublimated vapor remains in the envelope, it can expedite the onset of runaway gas accretion by increasing the mean molecular weight and decreases the adiabatic index of the gas (Brouwers and Ormel 2020).

However, if ices sublimate already in the planet's upper atmosphere the vapor could be transported back to the disk along with the gas (Wang et al. 2023; Steinmeyer et al. 2023). When this "volatice recycling" occurs, a compositional dichotomy may emerge: the planet retains the refractory elements from pebbles, while the disk gas becomes enriched in volatiles (Jiang et al. 2023).

Pebble accretion as a planet formation mechanism

Having established the basis of pebble accretion, we now turn to its ability to grow planets. A useful metric is the pebble accretion efficiency, which directly informs us on the required mass budget of pebbles. I will then discuss the different characteristics of pebble accretion in comparison to planetesimal accretion.

The Pebble accretion efficiency

Pebble accretion is not necessarily efficient. With this I mean that the *probability* of a pebble to be accreted:

$$\varepsilon \simeq \frac{\dot{m}}{\dot{M}_{\text{flux}}} = \mathcal{R}_{\text{peb}} \times \frac{v_K}{2\pi v_r} \tag{25}$$

can be low even though the rate ($\dot{m}$) is high. For example, when $\dot{M}_{\text{flux}} = 10^3 \, \text{m}_\oplus \, \text{Myr}^{-1}$, and $\varepsilon = 0.01$ a planet of 10 Earth mass doubles its mass after 1 Myr. But during this time an amount $990 \, m_\oplus$ in pebbles have drifted past the planets and are no longer available to its growth. This loss would be ameliorated if multiple embryos reside in the disk, but ε still captures the viability of pebble accretion to produce planets. After all, for planet formation to be successful, the preferred situation is that a few bodies consumes *most* of the pebbles, not that all pebbles get distributed over thousands of embryos.

The last step of Eq. (25), inserting $\dot{M}_{\text{flux}} = 2\pi r v_r \Sigma$ for the pebble flux, expresses ε in terms of the dimensionless accretion rates presented before (e.g., Table 1) and the radial drift expression (Eq. 6). Hence, ε can be expressed in terms of dimensionless quantities, $\varepsilon = \varepsilon(q, \tau_s, h_{\text{gas}}, \dots)$. Table 1 also lists ε in the 2D and 3D limits. In addition, we can define a mass

$$M_{\text{needed}} = \frac{m}{\varepsilon} = t_{\text{growth}} \dot{M}_{\text{flux}} \tag{26}$$

as the typical mass in pebbles required to grow a planet beyond mass m. In Fig. 5 this quantity is plotted in units of Earth masses for a solar-mass star and t_{growth} assumes a mass flux of $100 \, m_\oplus \, \text{yr}^{-1}$. In calculating ε we have used expressions and fits applicable for both small and large pebbles (Liu and Ormel 2018; Ormel and Liu 2018; Huang and Ormel 2023) as well as the expressions above for the isolation mass. The pebble scaleheight is calculated according to Dubrulle et al. (1995)

$$h_{\text{peb}} = \sqrt{\frac{\delta_z}{\delta_z + \tau_s}} h_{\text{gas}} \tag{27}$$

where δ_z represents the turbulent diffusivity normalized by c_s^2/Ω_K.

In Fig. 5a we can identify the accretion regimes outlined in Fig. 3. It shows that growth by ballistic accretion of pebbles in the Safronov limit is inefficient to impossible and that growth greatly accelerates for masses beyond the m_{init} threshold. The adopted parameters approximately correspond to conditions at 5 au and show that in order to grow an Earth-mass planet from a Lunar-mass embryo, a total amount of at least $75 \, m_\oplus$ pebbles are needed and that accretion can be fast. This renders pebble accretion potent, but far from efficient. Figure 5a also shows that smaller τ_s pebbles are more efficient building blocks than $\tau_s \sim 1$ pebbles; due to the former's reduced drift it is more likely they encounter the planet. Large pebbles ($\tau_s > 1$) would accrete even better as they settle into a thin layer. If they can be present in sufficiently large numbers they are arguably the most potent accretors.
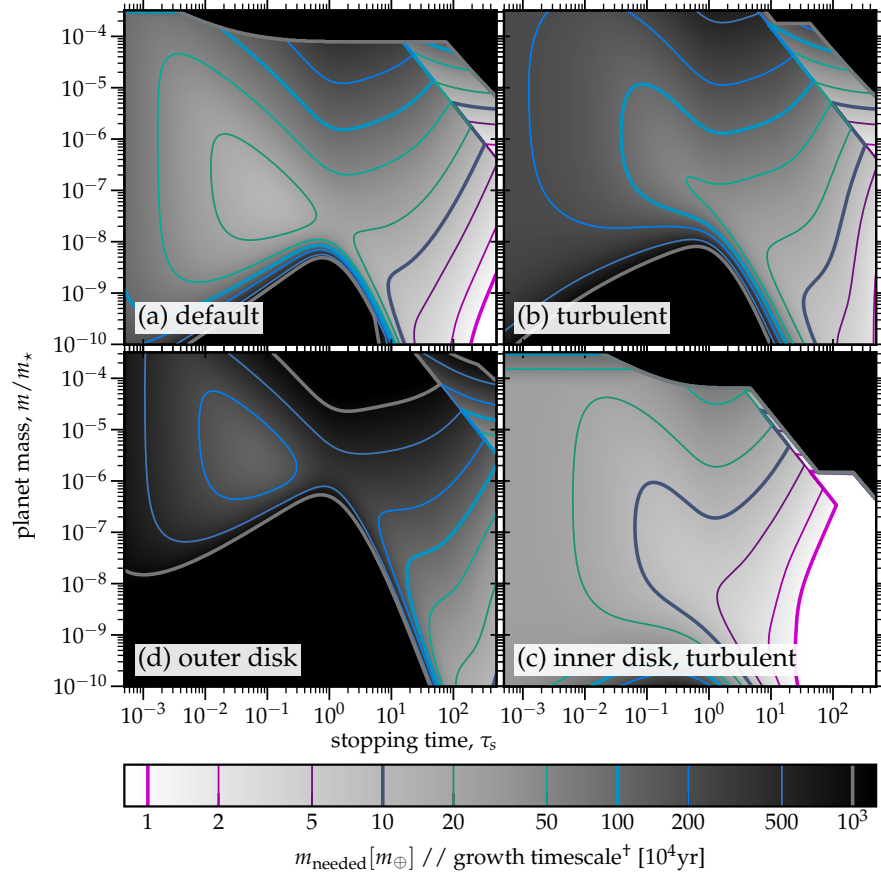
Fig. 5 Required pebble mass $M_{needed} = m/\varepsilon$ and growth timescale t_{growth} for pebble-accreting protoplanets. Contour levels assume a solar-mass star and a pebble flux of $100\,m_\oplus\,\mathrm{Myr}^{-1}$, in which case M_{needed} expressed in Earth units is equal to t_{growth} expressed in units of 10^4 yr. Contour labels are proportional to stellar mass and (for the growth timescale) inversely proportional to the pebble mass flux $\dot{M}_{flux}$. In (a) the efficiency has been calculated for $\delta_z = 10^{-4}$, $\eta = 5 \times 10^{-3}$, $h_{gas} = 0.05$ and $\alpha_R = 10^{-3}$, representing conditions at 5 au. (b) Turbulent disk at 5 au. (c) Inner disk, also turbulent. (d) The outer disk. Here, *turbulent* implies that $\delta_z = 10^{-2}$; *inner disk* that $\alpha_R = 2 \times 10^{-2}$, $h_{gas} = 0.03$, and $\eta = 10^{-3}$; and *outer disk* that $h_{gas} = 0.1$, $\eta = 2 \times 10^{-2}$, and $\alpha_R = 10^{-4}$.

The other panels in Fig. 5 illustrate how M_{needed} depends on the disk properties encapsulated by the parameters δ_z, α_R, h_{gas} and η. In Fig. 5b it can be seen that a more turbulent disk increases M_{needed} considerably for small τ_s, reflecting a shift towards 3D accretion. In the inner disk (Fig. 5c) accretion efficiencies are much higher, even for small τ_s, because h_{gas} and (in particular) η are lower. *In situ* formation of super-Earths/sub-Neptunes is an option. We also see in Fig. 5c that ballistic accretion of large pebbles ($\tau_s \gtrsim 10$) is much more efficient, because the smaller Hill radius (higher α_R) increases the probability of a hit.

Table 2 Asymptotic expressions for planetesimal accretion rates.

	2D limit	3D limit	validity
geometrical	$1.1\alpha_R e q^{1/3}$	$0.37\dfrac{\alpha_R^2 e q^{2/3}}{i}$	
dispersion	$2.4\alpha_R^{1/2} q^{2/3}$	$(1.5\text{--}1.9)\dfrac{\alpha_R q^{4/3}}{ie}$	$e \lesssim q^{1/3}\alpha_R^{-1/2}$
d.d., $\beta = 1/2$		$6.2\dfrac{\alpha_R q^{2/3}}{e_H^2}$	
shear	$5.4\alpha_R^{1/2} q^{2/3}$	$6.2\dfrac{\alpha_R q}{i}$	$e \lesssim q^{1/3}$

Notes. Accretion rates are given in units of $\Sigma r^2 \Omega$ in terms of: e (planetesimal eccentricity), i (planetesimal inclination), $q = m/m_\star$, $\alpha_R = R/R_{\mathrm{Hill}}$. Expressions for the geometrical and dispersion-dominated (d.d.) limit follow Greenzweig and Lissauer (1990) and are *not* averaged over a velocity distribution. In the 3D limit the numerical prefactor decreases from 1.9 at $\beta = i/e \ll 1$ to 1.5 at $\beta = 0.5$. For $\beta = 0.5$ we also provide the 3D, dispersion-dominated expression in terms of Hill eccentricity $e_H = (3/q)^{1/3}e$, which is by definition >1 in this limit. The shear-dominated (s.d.) expressions follow Ida and Nakazawa (1989) and Inaba et al. (2001).

In the far outer disk (Fig. 5d) pebble accretion becomes increasingly inefficient, even though with $\delta_z = 10^{-4}$ the disk is relatively quiescent. The pebble accretion onset mass m_{init} amounts to bodies similar to Pluto, if not Mars. This suppression of pebble accretion is entirely due to the higher η ($m_* \propto \eta^3 \propto h_{\mathrm{gas}}^6$) and therefore sensitive to the disk model. To render pebble accretion efficient the pebbles' drift velocity must be reduced, which can happen in rings (see below).

Comparison to Planetesimal Accretion

A frequently-discussed topic is how pebble accretion fares against planetesimal accretion. Unfortunately, this question depends strongly on the amount of accreting material present (Σ—now split over planetesimals or pebbles) and addressing the question which accretion mechanism dominates greatly depends on the disk model. It is therefore largely a matter of comparing apples to oranges. Still I will make a few comments.

In Table 2 I have compiled the specific *planetesimal* accretion rates in the same way as the accretion rates for pebble accretion (Table 1). One may see similarities between the expressions with $\alpha_R = R/R_H$ taking the role of τ_s and the planetesimal's inclination i taking the role of the pebble aspect ratio. For planetesimal-driven growth it is the 3D, dispersion-dominated limit that usually applies, with the collisional cross section enhanced by the Safronov factor $\Theta = (v_{\mathrm{esc}}/\Delta v)^2$. A key characteristics of planetesimal accretion is that the planetesimal eccentricity grows along with the planet's mass (viscous stirring), causing growth to slow down with increasing mass, i.e., the $4/3$ power dependence of $\dot{m}$ on q is misleading as e and i increase

concommitently. Specifically, the pebble and planetesimal growth timescales, assuming the dispersion-dominated (for planetesimals) and 3D limit (for pebbles) are:

$$t_{\mathrm{grw-pebbles}}^{3D} = 0.21 \frac{m_\star}{\Sigma_{\mathrm{peb}} r^2} \frac{h_{\mathrm{peb}}}{\tau_s} \Omega^{-1} \tag{28}$$

$$t_{\mathrm{grw-pltsm}}^{\mathrm{d.d.}} = 0.16 \frac{m_\star}{\Sigma_{\mathrm{pltsm}} r^2} \frac{q^{1/3} e_H^2}{\alpha_R} \Omega^{-1} \tag{29}$$

where $e_H \equiv e v_K / v_H = e (3/q)^{1/3}$ is the Hill eccentricity, which could range from ≈ 5 in the inner disk to ≈ 10 in the outer disk, dependent on gas density and planetesimal size (Kokubo and Ida 2002). Eccentricities can become even higher when gravitational stirring by turbulence-induced density inhomogeneities becomes important (Ida et al. 2008; Ormel and Okuzumi 2013). For pebble accretion, turbulent aerodynamical diffusion increases t_{grw} through increasing h_{peb} up to the point where it approaches the gas scaleheight.

In the inner disk, both Eqs. (28) and (29) will typically evaluate to values less than the disk lifetime. The excitation state of planetesimals will not matter too much, because the growth timescale, which we can also write as

$$t_{\mathrm{growth}} = \frac{m}{\dot{m}} \sim \frac{q^{1/3}}{\alpha_R^2 \Theta} \frac{m_\star}{\Sigma r^2} \Omega^{-1} \tag{30}$$

evaluates to $\sim 1\,\mathrm{Myr}$ for an Earth-mass planet at $\Sigma r^2 / m_\star = 10^{-4}$, even without focussing ($\Theta = 1$). The ability to grow by pebbles depends greatly on the size of the pebbles, which in the inner disk have lost their ice and could be much smaller *if* the fragmentation threshold correspondingly drops (but this is disputed; Musiolik and Wurm 2019). Although Fig. 5c suggests planets can form from (small) pebbles, the elephant in the room is whether the pebble flux can be maintained. The pebbles mass reservoir lies usually resides in the outer disk. Any "obstacle"—e.g., pressure bump, planetesimal belt (Guillot et al. 2014), or pebble-accreting planets upstream—would prevent these pebbles from reaching the inner disk.

In the outer disk Eqs. (28) and (29) show that pebble accretion is more powerful than planetesimal accretion, for the following reasons (i) τ_s usually is not too small; (ii) α_R is low, unless atmospheric capture of planetesimals is important; and (iii) Hill eccentricities of planetesimals are higher due to reduced gas damping. The main obstacles for pebble accretion are again the rather low efficiencies and the initiation mass threshold (Eq. 19). It is a matter of some debate whether a planetesimal formation mechanism such as the streaming instability can produce sufficiently massive bodies to meet the R_{init} threshold—at 40 au this would amount to Pluto-mass. Perhaps, after planetesimal *formation*, growth was first driven by planetesimal accretion, until the point where planets have become big enough to accrete pebbles (Levison et al. 2015a; Liu et al. 2019b; Alibert et al. 2018; Schoonenberg et al. 2019; Bitsch and Izidoro 2023; Jiang and Ormel 2023).

One environment where pebble accretion clearly stands out are particle-loaden rings, as seen with ALMA. The concentration of pebbles inside these rings could

be due to pressure maxima ($\eta \approx 0$) or due to particle pileups ($Z_{\mathrm{mid}} \gg 1$). In both cases pebbles travel on Keplerian orbits and Δv is much reduced, such that the R_{init} thresholds becomes a lesser issue. Accretion proceeds in the 2D limit at rates that will be extremely rapid:

$$t_{\mathrm{grw-pebbles}}^{\mathrm{2d,shear}} = 0.059\,\mathrm{Myr}\,\frac{\delta_w}{\tau_s^{2/3}}\left(\frac{m}{m_\oplus}\right)^{1/3}\left(\frac{M_{\mathrm{ring}}}{10\,m_\oplus}\right)^{-1}\left(\frac{m_\star}{m_\odot}\right)^{-5/6}\left(\frac{r}{50\,\mathrm{au}}\right)^{3/2}$$
(31)

where we used Eq. (15) and assumed the ring contains a mass M_{ring} in pebbles spread out over an annulus of width $\delta_w r$. This shows planets can form, by pebble accretion, at the distances where direct imaging planets are observed. While planetesimal-loaden rings in the inner disk would be able to spawn planets, only pebble accretion is a viable mechanism to do so in the outer disk (Lee et al. 2022; Jiang and Ormel 2023).

Application

Pebble accretion has been applied in a variety of settings. In the solar system, it is invoked to explain the emergence and architecture of the gas and ice giants (Levison et al. 2015a), the masses and compositions of the inner solar system planets (Levison et al. 2015b; Johansen et al. 2021), as well as the properties of the Jovian satellite system (Shibaike et al. 2019; Ronnet and Johansen 2020). Pebble accretion has been proposed to explaining specific exoplanet systems, such as TRAPPIST-1 (Schoonenberg et al. 2019), and circumbinary planets such as Kepler-16 (Coleman et al. 2023). Recently, it has been suggested to be responsible for certain features in protoplanetary disks, such as the compositional makeup of molecular rings (Jiang et al. 2023) and the sharpness of continuum rings (Huang et al. 2024). Finally, pebble accretion is invoked to explain the statistical properties of exoplanets using planet population synthesis approaches (Bitsch et al. 2019; Lambrechts et al. 2019; Liu et al. 2019a; Venturini et al. 2024).

A complete review of these and other works is beyond the scope of this chapter. I refer the interested reader to recent review articles by, for instance, Liu and Ji (2020) and Drążkowska et al. (2023).

Conclusion

With this concise review I aim to have clarified the following:

- Pebbles are defined in terms of the dimensionless stopping time τ_s: its aerodynamical size. Centered around $\tau_s = 1$, they are particles that drift over significant distances in disks.

- There is observational evidence that a large fraction of the solid mass budget in disks once existed in the form of pebble-sized particles.
- Pebble accretion requires a dissipative medium (gas). In the settling mechanism, particles are captured within the Hill sphere of the planet, from which they cannot escape. This contrast ballistic accretion, which relies on hitting a surface.
- The settling mechanism requires masses above an initiation mass m_{init} (Eq. 12) to ensure that encounters are sufficiently long. Pebble accretion (settling) is precluded below m_{init} and the settling condition will also start to fail for $\tau_s > 1$. There is an abrupt change in the accretion rate at m_{init}.
- Pebble accretion cross sections can be large, but in smooth disks growth is not necessarily efficient due to the strong drift of pebbles. A useful quantity to describe pebble accretion is the accretion probability ε.
- The pebble accretion rate is determined by the approach velocity Δv, the planet mass, τ_s, and the pebble scaleheight. These properties determine a variety of regimes (2D vs 3D; shear vs headwind), summarized in Fig. 3 and Table 1.
- Accretion of aerodynamically large pebbles ($\tau_s > 1$ but still drifting significantly) can become very effective as these particles settle to the midplane and approach at low velocity. Early planet atmospheres further boosts the accretion probability.
- In realistic situations, pebble accretion is likely to operate alongside planetesimal accretion. In the outer disk pebble accretion, once it is operational, is arguably more effective.
- Dense particulate rings, arising from local pressure maxima or particle pileups—likely the conditions of continuum rings seen with ALMA—can spawn planets through pebble accretion at large distances (several tens of au).

References

Alibert Y, Venturini J, Helled R et al. (2018) The formation of Jupiter by hybrid pebble-planetesimal accretion. Nature Astronomy 2:873–877

Ansdell M, Williams JP, Manara CF et al. (2017) An ALMA Survey of Protoplanetary Disks in the σ Orionis Cluster. AJ153:240

Ataiee S, Baruteau C, Alibert Y Benz W (2018) How much does turbulence change the pebble isolation mass for planet formation? A&A615:A110

Benítez-Llambay P Pessah ME (2018) Torques Induced by Scattered Pebble-flow in Protoplanetary Disks. ApJ855(2):L28

Birnstiel T, Andrews SM Ercolano B (2012) Can grain growth explain transition disks? A&A544:A79

Bitsch B Izidoro A (2023) Giants are bullies: How their growth influences systems of inner sub-Neptunes and super-Earths. A&A674:A178

Bitsch B, Lambrechts M Johansen A (2018) The growth of planets by pebble accretion in evolving protoplanetary discs (Corrigendum). A&A609:C2

Bitsch B, Izidoro A, Johansen A et al. (2019) Formation of planetary systems by pebble accretion and migration: growth of gas giants. A&A623:A88

Brouwers MG Ormel CW (2020) How planets grow by pebble accretion. II. Analytical calculations on the evolution of polluted envelopes. A&A634:A15

Brouwers MG, Vazan A Ormel CW (2018) How cores grow by pebble accretion. I. Direct core growth. A&A611:A65

Chrenko O, Chametla RO, Masset FS, Baruteau C Brož M (2024) Pebble-driven migration of low-mass planets in the 2D regime of pebble accretion. A&A690:A41

Cimerman NP, Kuiper R Ormel CW (2017) Hydrodynamics of embedded planets' first atmospheres - III. The role of radiation transport for super-Earth planets. MNRAS471:4662–4676

Coleman GAL, Nelson RP Triaud AHMJ (2023) Global N-body simulations of circumbinary planet formation around Kepler-16 and -34 analogues I: Exploring the pebble accretion scenario. MNRAS522(3):4352–4373

Dones L Tremaine S (1993) On the origin of planetary spins. Icarus103:67–92

Drążkowska J, Bitsch B, Lambrechts M et al. (2023) Planet Formation Theory in the Era of ALMA and Kepler: from Pebbles to Exoplanets. In: Inutsuka S, Aikawa Y, Muto T, Tomida K Tamura M (eds) Astronomical Society of the Pacific Conference Series, Astronomical Society of the Pacific Conference Series, vol 534, p 717, DOI 10.48550/arXiv.2203.09759

Dubrulle B, Morfill G Sterzik M (1995) The dust subdisk in the protoplanetary nebula. Icarus 114:237–246

Greenzweig Y Lissauer JJ (1990) Accretion rates of protoplanets. Icarus 87:40–77

Guerra-Alvarado OM, Carrasco-González C, Macías E et al. (2024) Into the thick of it: ALMA 0.45 mm observations of HL Tau at a resolution of 2 au. A&A686:A298

Guillot T, Ida S Ormel CW (2014) On the filtering and processing of dust by planetesimals. I. Derivation of collision probabilities for non-drifting planetesimals. A&A572:A72

Hasegawa M Nakazawa K (1990) Distant encounter between Keplerian particles. A&A227:619–627

Huang H Ormel CW (2023) Accretion of aerodynamically large pebbles. MNRAS522(2):2241–2258

Huang S, van der Marel N Portegies Zwart S (2024) On the origin of transition disk cavities: Pebble-accreting protoplanets vs Super-Jupiters. arXiv e-prints arXiv:2410.02856

Ida S Nakazawa K (1989) Collisional probability of planetesimals revolving in the solar gravitational field. III. A&A224:303–315

Ida S, Guillot T Morbidelli A (2008) Accretion and Destruction of Planetesimals in Turbulent Disks. ApJ686:1292–1301

Inaba S Ikoma M (2003) Enhanced collisional growth of a protoplanet that has an atmosphere. A&A410:711–723

Inaba S, Tanaka H, Nakazawa K, Wetherill GW Kokubo E (2001) High-Accuracy Statistical Simulation of Planetary Accretion: II. Comparison with N-Body Simulation. Icarus 149:235–250

Jiang H Ormel CW (2023) Efficient planet formation by pebble accretion in ALMA rings. MNRAS518(3):3877–3900

Jiang H, Wang Y, Ormel CW, Krijt S Dong R (2023) Chemical footprints of giant planet formation. Role of planet accretion in shaping the C/O ratio of protoplanetary disks. A&A678:A33

Johansen A, Ida S Brasser R (2019) How planetary growth outperforms migration. A&A622:A202

Johansen A, Ronnet T, Bizzarro M et al. (2021) A pebble accretion model for the formation of the terrestrial planets in the Solar System. Science Advances 7(8):eabc0444

Kataoka A, Muto T, Momose M et al. (2015) Millimeter-wave Polarization of Protoplanetary Disks due to Dust Scattering. ApJ809:78

Kobayashi H, Tanaka H Krivov AV (2011) Planetary Core Formation with Collisional Fragmentation and Atmosphere to Form Gas Giant Planets. ApJ738:35–+

Kokubo E Ida S (2002) Formation of Protoplanet Systems and Diversity of Planetary Systems. ApJ581:666–680

Kuwahara A Kurokawa H (2020a) Influences of protoplanet-induced three-dimensional gas flow on pebble accretion. I. Shear regime. A&A633:A81

Kuwahara A Kurokawa H (2020b) Influences of protoplanet-induced three-dimensional gas flow on pebble accretion. II. Headwind regime. A&A643:A21

Kuwahara A Kurokawa H (2024) Analytic description of the gas flow around planets embedded in protoplanetary disks. A&A682:A14

Lambrechts M Johansen A (2012) Rapid growth of gas-giant cores by pebble accretion. A&A544:A32

Lambrechts M, Morbidelli A, Jacobson SA et al. (2019) Formation of planetary systems by pebble accretion and migration. How the radial pebble flux determines a terrestrial-planet or super-Earth growth mode. A&A627:A83

Lee EJ, Fuentes JR Hopkins PF (2022) Establishing Dust Rings and Forming Planets within Them. ApJ937(2):95

Levison HF, Kretke KA Duncan MJ (2015a) Growing the gas-giant planets by the gradual accumulation of pebbles. Nature524:322–324

Levison HF, Kretke KA, Walsh KJ Bottke WF (2015b) Growing the terrestrial planets from the gradual accumulation of sub-meter sized objects. Proceedings of the National Academy of Science 112:14,180–14,185

Liu B Ji J (2020) A tale of planet formation: from dust to planets. Research in Astronomy and Astrophysics 20(10):164

Liu B Ormel CW (2018) Catching drifting pebbles. I. Enhanced pebble accretion efficiencies for eccentric planets. A&A615:A138

Liu B, Lambrechts M, Johansen A Liu F (2019a) Super-Earth masses sculpted by pebble isolation around stars of different masses. A&A632:A7

Liu B, Ormel CW Johansen A (2019b) Growth after the streaming instability. From planetesimal accretion to pebble accretion. A&A624:A114

Lyra W, Johansen A, Cañas MH Yang CC (2023) An Analytical Theory for the Growth from Planetesimals to Planets by Polydisperse Pebble Accretion. ApJ946(2):60

Musiolik G Wurm G (2019) Contacts of Water Ice in Protoplanetary Disks—Laboratory Experiments. ApJ873(1):58

Muto T Inutsuka S (2009) Orbital Evolution of a Particle Interacting with a Single Planet in a Protoplanetary Disk. ApJ695:1132–1150

Nakagawa Y, Sekiya M Hayashi C (1986) Settling and growth of dust particles in a laminar phase of a low-mass solar nebula. Icarus 67:375–390

Okamura T Kobayashi H (2021) The Growth of Protoplanets via the Accretion of Small Bodies in Disks Perturbed by the Planetary Gravity. ApJ916(2):109

Ormel CW Klahr HH (2010) The effect of gas drag on the growth of protoplanets. Analytical expressions for the accretion of small bodies in laminar disks. A&A520:A43

Ormel CW Liu B (2018) Catching drifting pebbles. II. A stochastic equation of motion for pebbles. A&A615:A178

Ormel CW Okuzumi S (2013) The Fate of Planetesimals in Turbulent Disks with Dead Zones. II. Limits on the Viability of Runaway Accretion. ApJ771:44

Ormel CW, Kuiper R Shi JM (2015) Hydrodynamics of embedded planets' first atmospheres - I. A centrifugal growth barrier for 2D flows. MNRAS446:1026–1040

Ronnet T Johansen A (2020) Formation of moon systems around giant planets. Capture and ablation of planetesimals as foundation for a pebble accretion scenario. A&A633:A93

Sanchis E, Testi L, Natta A et al. (2021) Measuring the ratio of the gas and dust emission radii of protoplanetary disks in the Lupus star-forming region. A&A649:A19

Schneider AD Bitsch B (2021) How drifting and evaporating pebbles shape giant planets. I. Heavy element content and atmospheric C/O. A&A654:A71

Schoonenberg D, Liu B, Ormel CW Dorn C (2019) Pebble-driven planet formation for TRAPPIST-1 and other compact systems. A&A627:A149

Shibaike Y, Ormel CW, Ida S, Okuzumi S Sasaki T (2019) The Galilean Satellites Formed Slowly from Pebbles. ApJ885(1):79

Sierra A, Pérez LM, Zhang K et al. (2021) Molecules with ALMA at Planet-forming Scales (MAPS). XIV. Revealing Disk Substructures in Multiwavelength Continuum Emission. ApJS257(1):14

Steinmeyer ML, Woitke P Johansen A (2023) Sublimation of refractory minerals in the gas envelopes of accreting rocky planets. A&A677:A181

Takaoka K, Kuwahara A, Ida S Kurokawa H (2023) Spin of protoplanets generated by pebble accretion: Influences of protoplanet-induced gas flow. A&A674:A193

Testi L, Birnstiel T, Ricci L et al. (2014) Dust Evolution in Protoplanetary Disks. Protostars and Planets VI pp 339–361

Tychoniec Ł, Manara CF, Rosotti GP et al. (2020) Dust masses of young disks: constraining the initial solid reservoir for planet formation. A&A640:A19

Venturini J, Alibert Y, Benz W Ikoma M (2015) Critical core mass for enriched envelopes: the role of H_2O condensation. A&A576:A114

Venturini J, Ronco MP, Guilera OM et al. (2024) A fading radius valley towards M dwarfs, a persistent density valley across stellar types. A&A686:L9

Visser RG Ormel CW (2016) On the growth of pebble-accreting planetesimals. A&A586:A66

Visser RG, Ormel CW, Dominik C Ida S (2020) Spinning up planetary bodies by pebble accretion. Icarus335:113380

Wang Y, Ormel CW, Huang P Kuiper R (2023) Atmospheric recycling of volatiles by pebble-accreting planets. MNRAS523(4):6186–6207

Weidenschilling SJ (1997) The Origin of Comets in the Solar Nebula: A Unified Model. Icarus 127:290–306

Weidenschilling SJ Davis DR (1985) Orbital resonances in the solar nebula - Implications for planetary accretion. Icarus 62:16–29

Wentworth CK (1922) A Scale of Grade and Class Terms for Clastic Sediments. Journal of Geology 30(5):377–392

Williams S, Arsenault M, Buczkowski B et al. (2006) Surficial sediment character of the Louisiana offshore Continental Shelf region: a GIS Compilation. US Geological Survey Open-File Report 2006-1195 URL http://pubs.usgs.gov/of/2006/1195/index.htm

Yang H, Li ZY, Looney L Stephens I (2016) Inclination-induced polarization of scattered millimetre radiation from protoplanetary discs: the case of HL Tau. MNRAS456(3):2794–2805